Finite Element Analysis and Optimization of a Single-Axis Acoustic Levitator

Marco A. B. Andrade, Flávio Buiochi, and Julio C. Adamowski

***Abstract*—A finite element analysis and a parametric optimization of single-axis acoustic levitators are presented. The finite element method is used to simulate a levitator consisting of a Langevin ultrasonic transducer with a plane radiating surface and a plane reflector. The transducer electrical impedance, the transducer face displacement, and the acoustic radiation potential that acts on small spheres are determined by the finite element method. The numerical electrical impedance is compared with that acquired experimentally by an impedance analyzer, and the predicted displacement is compared with that obtained by a fiber-optic vibration sensor. The numerical acoustic radiation potential is verified experimentally by placing small spheres in the levitator. The same procedure is used to optimize a levitator consisting of a curved reflector and a concave-faced transducer. The numerical results show that the acoustic radiation force in the new levitator is enhanced 604 times compared with the levitator consisting of a plane transducer and a plane reflector. The optimized levitator is able to levitate 3, 2.5-mm diameter steel spheres with a power consumption of only 0.9 W.**

I. Introduction

Acoustic levitation has been used in many research areas, such as measurement of liquid surface tension [1], trapping of heavy gases [2], formation of ice particles in stationary ultrasonic fields [3], [4], and analytical and bioanalytical chemistry [5]. Different techniques have been proposed to levitate particles, including magnetic levitation [6], optical levitation [7], and electrostatic levitation [8], [9]. The main advantage of acoustic levitation over other levitation techniques is that it does not have any special restriction on the levitated particle, such as its electric or magnetic properties. Therefore, acoustic levitation is suitable to levitate aqueous droplets and nonmetallic substances.

The simplest acoustic levitator is called single-axis acoustic levitator and consists of an ultrasonic transducer and a reflector. Many single-axis acoustic levitators use a Langevin-type transducer [10], [11] to generate a standing wave between the transducer and the reflector. This type of transducer is formed by pairs of piezoelectric rings sandwiched between 2 loading masses and prestressed by a central bolt.

Manuscript received August 20, 2009; accepted October 23, 2009. This work was supported by the following Brazilian sponsor agencies: CNPq, CAPES, and Petrobras/ANP.

The authors are with the Mechatronics Engineering Department, Escola Politécnica da Universidade de São Paulo, São Paulo, Brazil (e-mail: marcobrizzotti@gmail.com).

Digital Object Identifier 10.1109/TUFFC.2010.1427

The applications involving acoustic levitation require knowledge of the acoustic forces that act on the levitated object. One of the first works dealing with the acoustic radiation force on spheres was presented by King [12]. In his work, King presented a theoretical study on the force that acts on a rigid sphere in a standing wave field. Some decades later, Gor'kov [13] derived a method to calculate the acoustic radiation potential that acts on a small sphere in an arbitrary acoustic field. Barmatz and Collas [14] applied the method of Gor'kov for deriving the acoustic radiation potential on a sphere for rectangular, cylindrical, and spherical standing wave fields. Because the geometries used by Barmatz and Collas are simple, the acoustic radiation potential is given by an analytical solution. More recently, Xie and Wei [15], [16] used the boundary element method and the Gor'kov expression to study the influence of the geometrical parameters on a single-axis levitator. With this study, they designed a levitator that is able to levitate small living animals [17] and heavy tungsten balls [18]. An interesting approach to simulate an acoustic levitator was presented by Kozuka *et al.* [19]. In their work, the Rayleigh integral was used with multiple reflected waves between the transducer and the reflector to determine the standing wave acoustic field.

The numerical models commonly used in the design of acoustic levitators require the previous knowledge of the displacement distribution on the transducer face. Therefore, the complete levitator analysis requires at least 2 steps. First, a numerical model is used to determine the transducer displacement amplitudes. Then, these displacements are used in another numerical model to determine the acoustic radiation potential that acts on the levitated object. Aiming at modeling the entire acoustic levitator, this work presents a finite element analysis of a single-axis acoustic levitator consisting of a piezoelectric transducer and a plane reflector. Due to the levitator circular geometry, axisymmetric elements are used to reduce the computational time. The proposed model is also used to design a curved reflector and a new transducer with a concave radiating surface that maximizes the acoustic force on the levitated object. The simulation of the acoustic levitator includes the fluid-structure interaction between the transducer and air and the coupling between the electrical and mechanical properties of the piezoelectric material.

II. Numerical Modeling

The single-axis acoustic levitator used in this work consists of a 19.9-kHz transducer and a plane stainless steel

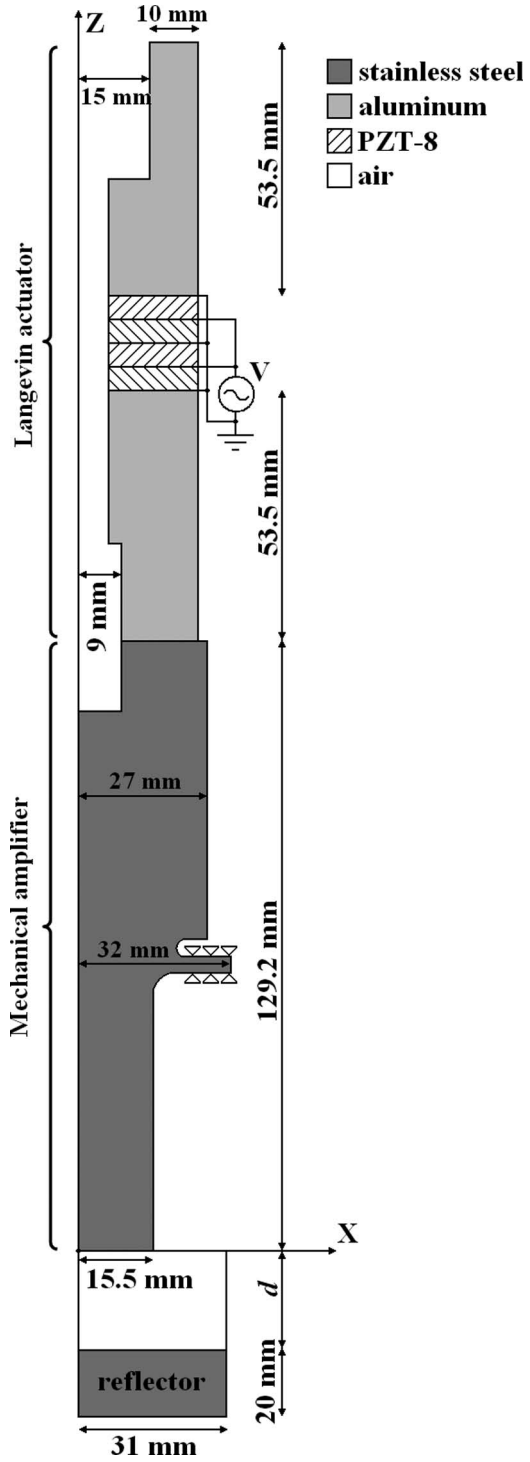

Fig. 1. Two-dimensional axysimmetric model of the single-axis acoustic levitator.

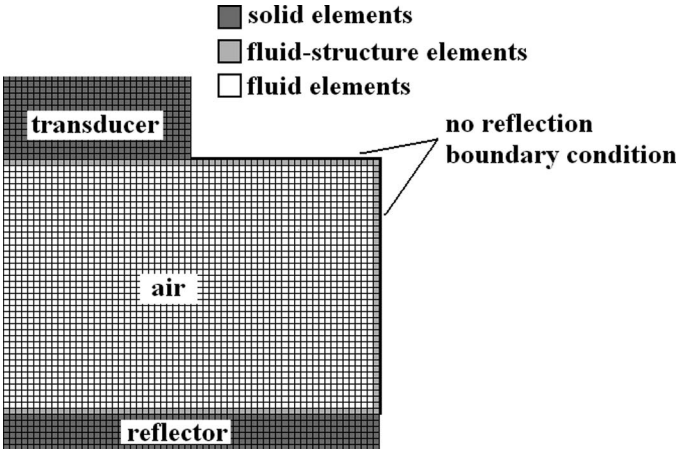

Fig. 2. Boundary conditions used in the region between the transducer and the reflector.

reflector. The transducer consists of a Langevin-type actuator, which is formed of 4 piezoelectric ceramic rings sandwiched between 2 aluminum loading masses and a steel mechanical amplifier. Each piezoelectric ceramic is made of lead zirconate titanate (PZT-8) with 5-mm thickness, 50-mm external diameter, and 15-mm internal diameter. Each adjacent pair of piezoelectric rings has polarization in opposite directions. The schematic of the single-axis acoustic levitator is shown in Fig. 1. In this figure, the coordinate x corresponds to the radial direction, and d is the distance between the transducer and the reflector.

The simulation of the entire levitator, including the piezoelectric transducer, can help toward the design of complex shape acoustic levitators. To study the levitator behavior, the finite element package ANSYS (ANSYS Inc., Canonsburg, PA) is used for simulation. In ANSYS, a harmonic analysis is conducted in the frequency range from 19.7 kHz to 20.3 kHz. Zero displacement boundary conditions are applied to the nodes in the center of the mechanical amplifier. Zero displacements are represented by triangles and electrical boundary conditions are represented by the voltage source V in Fig. 1. In ANSYS, a piezoelectric coupled-field element is used to simulate the PZT-8. This type of element has displacement and voltage degrees of freedom. The modeling of loading masses, mechanical amplifier, and reflector is performed by using a structural element that has only displacement degrees-of-freedom in directions x and z. An acoustic fluid element is used to simulate the air region between the transducer and the reflector. This element has a pressure degree of freedom. The interaction between the mechanical parts and the air region is made by using fluid-structure elements that have displacement and pressure degrees of freedom. These elements are used in the interface between the mechanical parts and the air, as shown in Fig. 2. Fig. 2 also shows the no-reflection boundary condition, which simulates an infinite air region. In the finite element modeling, the mesh size is set to 0.5 mm. A rule of thumb says that it is necessary to use at least 20 elements per wavelength to ensure a good convergence. Therefore, a mesh size of 0.5 mm is enough to simulate the acoustic levitator, because the smallest wavelength occurs in air and one twentieth of a wavelength is equal to 0.83 mm.

The material properties used in the simulation are presented in Table I. The PZT properties were extracted from [20]. In this table, c_{ij}^{E} are the stiffness constants at constant electric field, e_{ij} are the piezoelectric coefficients, $\varepsilon_{ij}^{S}/\varepsilon_0$ are dielectric constants at constant strain, where

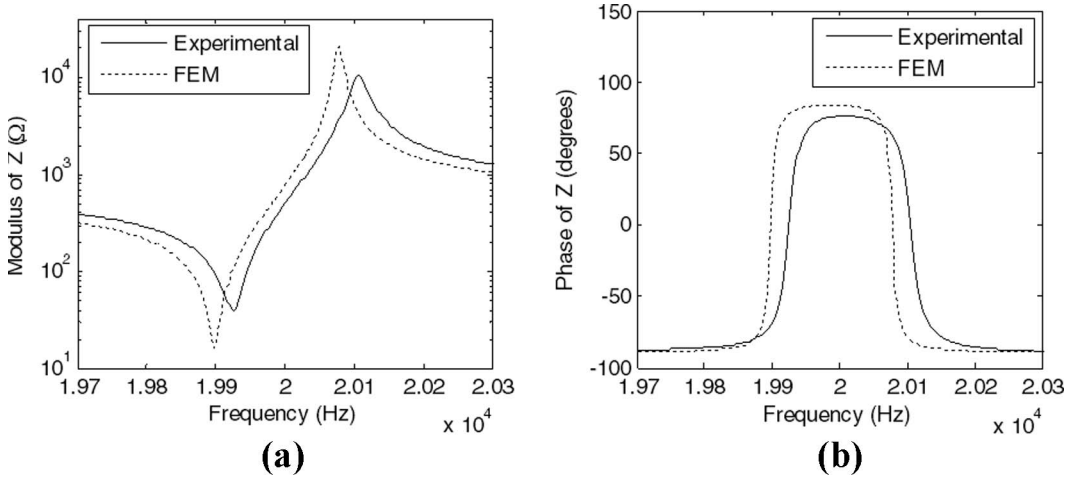

Fig. 3. Comparison between the numerical and experimental electrical impedance: (a) modulus and (b) phase.

TABLE I. MATERIAL PROPERTIES.

PZT-8	
$c_{11}^{E}(10^{10}\ \mathrm{N/m^2})$	13.7
$c_{12}^{E}(10^{10}\ \mathrm{N/m^2})$	6.97
$c_{13}^{E}(10^{10}\ \mathrm{N/m^2})$	7.16
$c_{33}^{E}(10^{10}\ \mathrm{N/m^2})$	12.4
$c_{44}^{E}(10^{10}\ \mathrm{N/m^2})$	3.14
$e_{31}\ (\mathrm{C/m^2})$	−4
$e_{33}\ (\mathrm{C/m^2})$	13.8
$e_{15}\ (\mathrm{C/m^2})$	10.4
$\varepsilon_{11}^{S}/\varepsilon_0$	898
$\varepsilon_{33}^{S}/\varepsilon_0$	582
$\rho\ (\mathrm{kg/m^3})$	7600
$\beta\ (10^{-10}\ \mathrm{s})$	30
Aluminum	
$E\ (10^{10}\ \mathrm{N/m^2})$	7.43
ν	0.33
$\rho\ (\mathrm{kg/m^3})$	2900
$\beta\ (10^{-10}\ \mathrm{s})$	40
Stainless steel	
$E\ (10^{10}\ \mathrm{N/m^2})$	20.8
ν	0.29
$\rho\ (\mathrm{kg/m^3})$	7850
$\beta\ (10^{-10}\ \mathrm{s})$	40
Air	
$\rho\ (\mathrm{kg/m^3})$	1.2
$c\ (\mathrm{m/s})$	340

$\varepsilon_0 = 8.85 \times 10^{-12}$ F/m is the permittivity of free space, ρ is the density, E is the Young modulus, ν is the Poisson ratio, c is the propagation velocity, and β is the damping.

The main characteristics of a transducer can be determined through its electrical impedance curve. The transducer electrical impedance is not directly provided by the ANSYS package. However, it can be calculated from the electrical charge given by the program. In ANSYS, the electrical charge $Q(t)$ on the piezoelectric ceramics electrodes is represented by

$$Q(t) = Q_0 \exp(-j\omega t), \tag{1}$$

where Q_0 is the complex electrical charge amplitude, ω is the angular frequency, and t is the time. The electrical current $I(t)$ is given by

$$I(t) = \frac{\mathrm{d}Q}{\mathrm{d}t} = -j\omega Q_0 \exp(-j\omega t) = -j\omega Q(t). \tag{2}$$

Finally, the electrical impedance Z is given by

$$Z = \frac{V}{I} = \frac{-V}{j\omega Q(t)}, \tag{3}$$

where V is the voltage applied to the electrodes of the piezoelectric ceramic.

After running the finite element method for a frequency range from 19.7 to 20.3 kHz, (3) was used to determine the electrical impedance curve of the ultrasonic transducer. To validate the numerical model, the transducer electrical impedance was measured by using an HP4194A (Hewlett Packard, Palo Alto, CA) impedance analyzer. The comparison between the numerical and experimental electrical impedance curve is presented in Fig. 3.

The finite element method is also used to determine the displacement in the center of the transducer face as a function of frequency. The validation of the numerical displacement is made by using an MTI-2100 fiber-optic vibration sensor (MTI Instruments, Inc., Albany, NY). The comparison between the numerical displacement and the measured displacement is presented in Fig. 4. These displacements were obtained by considering an excitation voltage amplitude of 1 V. Figs. 3 and 4 show that the numerical resonance frequency corresponds to 19.90 kHz and the measured resonance frequency corresponds to 19.92 kHz. To produce the maximum acoustic radiation force on the particle, the acoustic levitator should work at the resonance frequency. Because the transducer has a narrow bandwidth, a small error in the excitation frequency produces a large error in the transducer displacement amplitude. The finite element analysis also shows that the displacement distribution in the transducer face

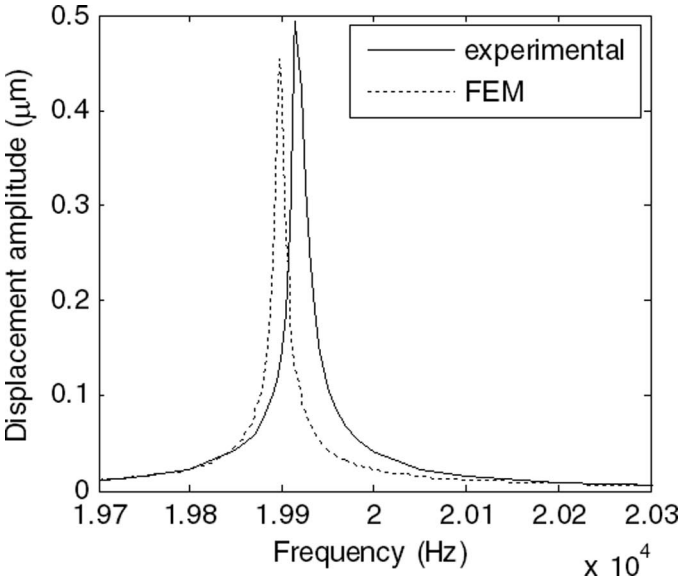

Fig. 4. Comparison between the numerical and experimental transducer face displacement.

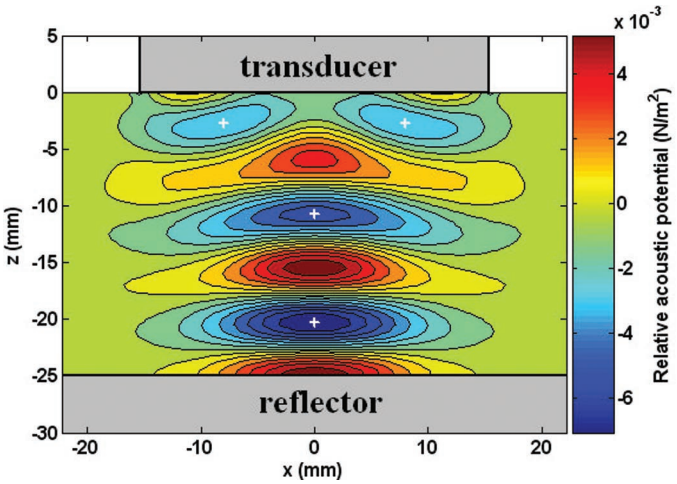

Fig. 5. Numerical acoustic radiation potential when the distance between the transducer and the plane reflector is 25.0 mm and when the transducer is excited with a 19.9-kHz sine wave.

can be considered uniform, because the highest displacement amplitude corresponds to 0.45 μm at the center of the transducer face and the smallest displacement is equal to 0.44 μm at the edge of the transducer face.

After determining the transducer resonance frequency, the finite element method is used to study the acoustic radiation force produced by the single-axis levitator. In this work, the forces that act on the levitated object are studied by using the Gor'kov theory [13]. The Gor'kov theory assumes that the particle size is much smaller than the wavelength. According to this theory, the forces that act on a sphere of radius R are modeled by the acoustic radiation potential U, given by

$$U = 2\pi R^3 \left(\frac{\overline{p^2}}{3\rho c^2} - \frac{\rho \overline{u^2}}{2} \right), \tag{4}$$

where $\overline{p^2}$ and $\overline{u^2}$ are the mean square amplitudes of the pressure and velocity, respectively, c is the propagation velocity in air, and ρ is the air density. The fluid element used to simulate the air in ANSYS provides the pressure distribution between the transducer and the reflector. The velocity field u, required by (4), is calculated by using the following equations [21]:

$$\phi = -\frac{p}{j\omega\rho} \tag{5}$$

$$u = \nabla\phi. \tag{6}$$

The relation between the acoustic radiation potential U and the force F that acts on the sphere is given by

$$F = -\nabla U. \tag{7}$$

The acoustic radiation potential depends on the radius of the levitated sphere. To determine a potential that is independent of the radius, a relative acoustic radiation potential $\tilde{U}$ and a relative acoustic radiation force $\tilde{F}$ are defined

$$\tilde{U} = \frac{U}{2\pi R^3} \tag{8}$$

$$\tilde{F} = -\nabla \tilde{U}. \tag{9}$$

The relative acoustic radiation potential was determined numerically for a distance d of 25 mm, and it is presented in Fig. 5. The positions where levitation can occur correspond to the positions of minimum acoustic potential. The positions of minimum acoustic potential are denoted by the symbol "+" in Fig. 5. Two of the potential minima are located along z-axis at positions $z = -20.25$ mm and $z = -10.75$ mm. The other potential minimum does not occur at the center of the levitator, and therefore it results in a ring-shaped potential well. This levitation point occurs at coordinates $x = 8.00$ mm and $z = -2.75$ mm and at $x = -8.00$ mm and $z = -2.75$ mm.

Fig. 6 presents the relation between $\tilde{U}$ and $\tilde{F}$ along z-axis. In this figure, there are many positions where the acoustic radiation force is zero. However, only the positions of minimum acoustic radiation potential are levitation points. Although there is a potential minimum in direction z at $z = -1.2$ mm, this point does not result in a levitation point, because it is a saddle point. When a particle is placed at this point, it migrates to the minimum potential point at $x = 8.00$ mm and $z = -2.75$ mm or to point $x = -8.00$ mm and $z = -2.75$ mm.

The behavior of a sphere in the neighborhood of a minimum potential is similar to the behavior of a harmonic oscillator. Therefore, an elastic constant can be defined in a neighborhood of a minimum potential:

$$\tilde{k} = \frac{\partial^2 \tilde{U}}{\partial z^2}. \tag{10}$$

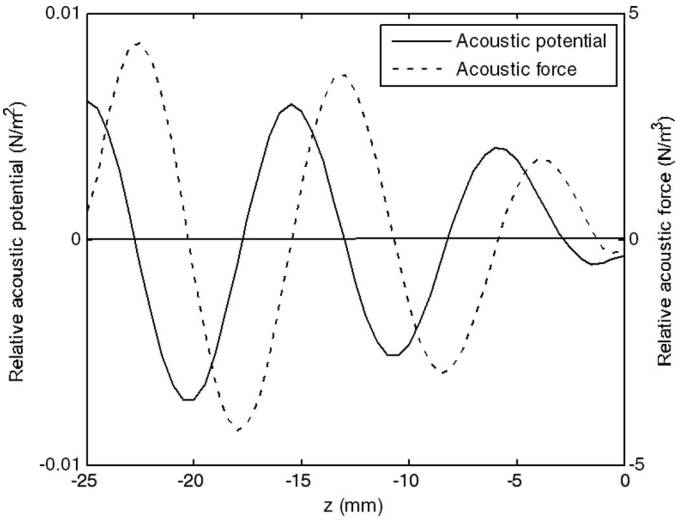

Fig. 6. Relative acoustic radiation potential and relative force along the z-axis when the distance between the transducer and reflector is 25.0 mm.

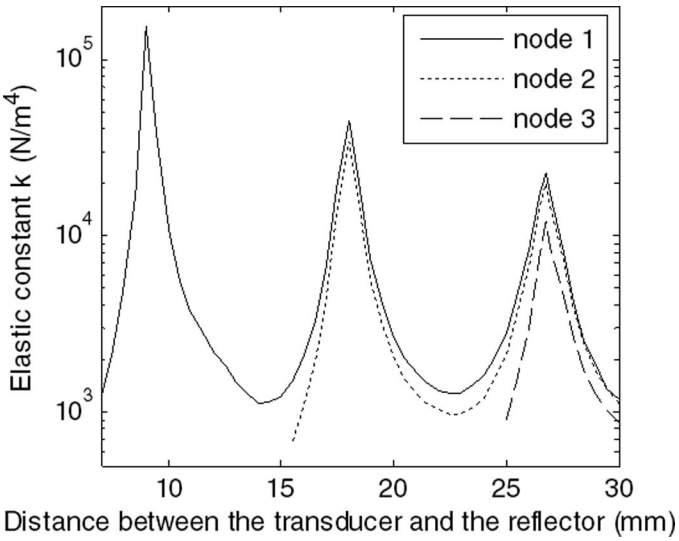

Fig. 7. Elastic constant as a function of distance d between the transducer and the reflector.

According to Barmatz and Collas [14], the elastic constant is useful for comparing the levitation capabilities of various potential minima. For a perfect rectangular geometry levitator, a maximum elastic constant is obtained when the distance between the transducer and the reflector is a multiple of half wavelength. Because this levitator does not have a rectangular geometry, many finite element simulations are done by changing the parameter d to determine the optimal distances between the transducer and the reflector. The elastic constant determined for each levitation point (node) along z-axis is presented in Fig. 7. When the distance between the transducer and the reflector is small, there is only one levitation point. If distance d is increased, other potential minima arise. According to Fig. 7, the optimal distances d for levitation are 9 mm, 18 mm, and 26.5 mm. The maximum restoring force occurs when the distance d is 9 mm. In this case, there is only one levitation point, and the elastic constant corresponds to 1.5×10^5 N/m^4. When the distance d is 18 mm, there are 2 levitation points, and the elastic constants correspond to 4.6×10^4 N/m^4 and 3.4×10^4 N/m^4 for the bottom and top nodes, respectively. For a distance d corresponding to 26.5 mm, the elastic constants are 2.3×10^4 N/m^4, 2.0×10^4 N/m^4 and 1.2×10^4 N/m^4, for the bottom, central, and top node, respectively. It can also be observed in Fig. 7, that the maximum elastic constant decreases when the number of levitation positions is increased. This result agrees with that obtained by Xie and Wei [16], who verified that the levitation force decreases when the distance between the transducer and the reflector is increased to create more levitation positions.

The positions of minimum acoustic potential determined by the finite element method were verified experimentally for the 3 optimal distances d. The experimental verification was done by placing small Styrofoam spheres between the transducer and the plane reflector. The Styrofoam spheres have a diameter in the order of 2 mm. The comparison between the numerical acoustic radiation potential and the equilibrium positions of the spheres is presented in Fig. 8. As shown in Fig. 8, the experimental equilibrium positions of the spheres are in good agreement with the minimum potential positions determined by the finite element method. It was verified that when the electrical voltage applied to the transducer is gradually reduced, the sphere that lies in the levitation position with the lowest elastic constant falls first.

III. Curved Reflector Design

Many authors, including [11], [15], [16], and [22], have used curved reflectors to increase the acoustic radiation force that acts on the levitated object. In this work, the finite element method is used to design a spherical reflector that optimizes the levitation force. It is considered that the reflector and the transducer are separated by a distance d, and that the reflector has a radius of curvature R, as shown in Fig. 9. Xie and Wei have verified that a reflector with a large depth can increase the force on the levitated particle; however, it is difficult to have access to the particle [16]. To avoid a levitator with a large depth curved reflector, the reflector external diameter was chosen to be 40 mm. To find the optimal parameters d and R, the finite element method is used to determine the relative elastic constant as a function of these 2 parameters. Because the displacement distribution in the transducer face can be considered uniform for this transducer, only the region between the transducer face and the reflector is simulated, as shown in Fig. 9. It is considered that the displacement amplitude in the transducer face is 0.45 μm. A harmonic analysis was conducted at 19.9 kHz over the domain 18 mm $\leq d \leq$ 20.5 mm, 25 mm $\leq R \leq$ 90 mm. This domain was chosen to create 2 potential minima between the transducer and the reflector, as in Figs. 8(c) and

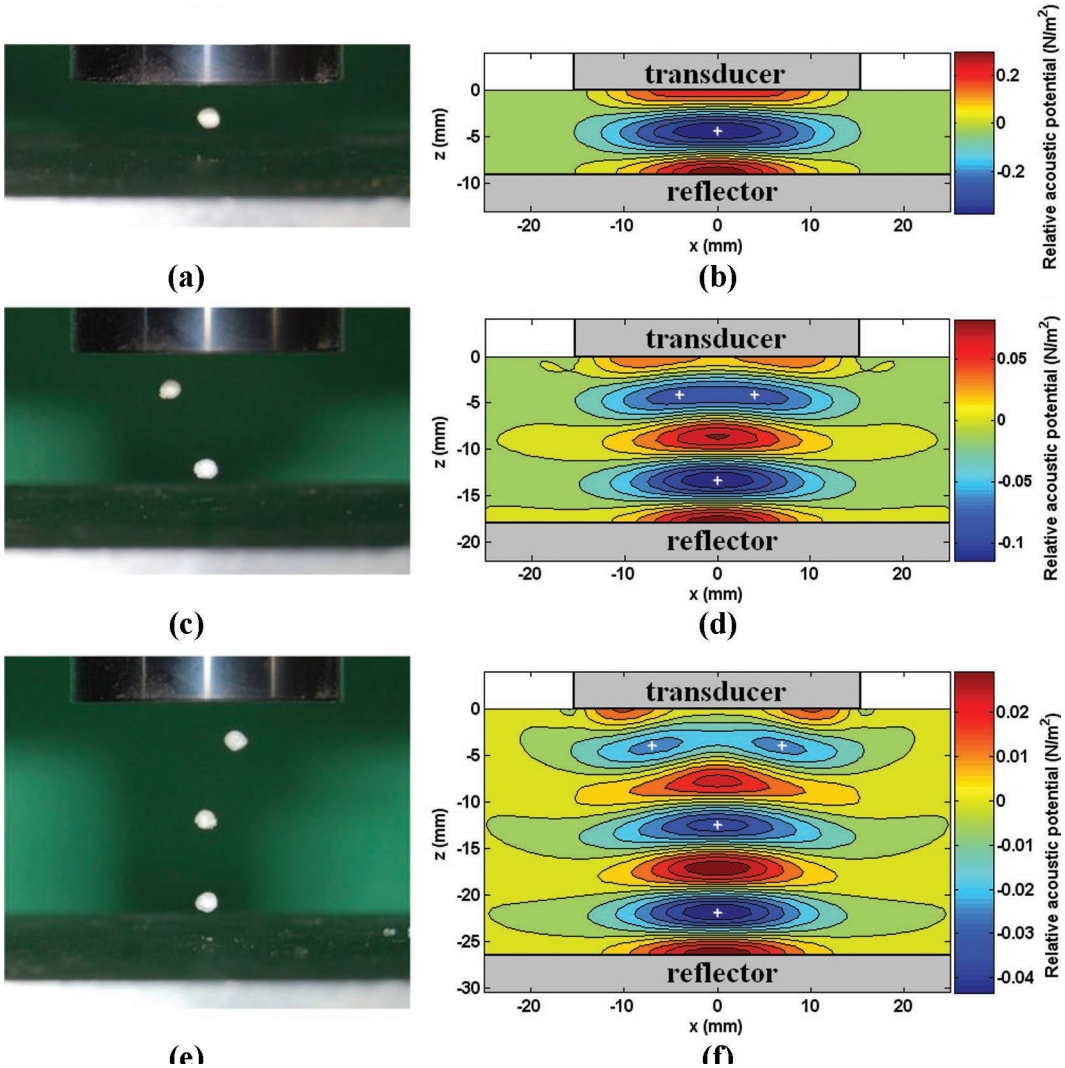

Fig. 8. Comparison between the numerical acoustic radiation potential and the levitation position of small Styrofoam spheres: (a) experimental ($d = 9$ mm); (b) numerical ($d = 9$ mm); (c) experimental ($d = 18$ mm); (d) numerical ($d = 18$ mm); (e) experimental ($d = 26.5$ mm); (f) numerical ($d = 26.5$ mm).

8(d). When both transducer and reflector have plane surface, the optimal distance d to create 2 levitation points corresponds to 18 mm and the curvature radius of the reflector can be assumed to be infinite. When the reflector radius of curvature decreases, it is necessary to increase the distance d, because the mean distance between the transducer and the reflector decreases with the increase of the radius of curvature. Therefore, a lower bound of 18 mm was chosen for distance d.

After determining the acoustic radiation potential through the finite element method for different values of d and R, the elastic constant in the neighborhood of the bottom acoustic potential minimum was determined and is shown in Fig. 10. According to this figure, the maximum elastic constant is obtained when distance d is approximately 19.5 mm, and the radius R is 30 mm. The elastic constant shown in Fig. 10 also shows that the distance between the transducer and the reflector cannot be determined by assuming that this distance is a multiple of half wavelength. For a given radius of curvature, it is

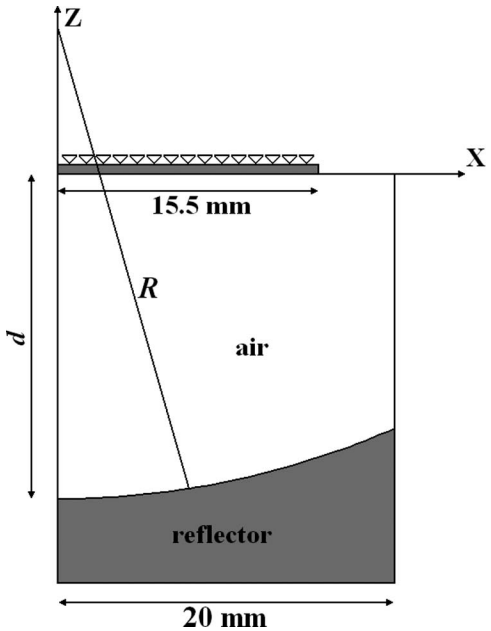

Fig. 9. Two-dimensional axysimmetric model of the single-axis acoustic levitator with a curved reflector.

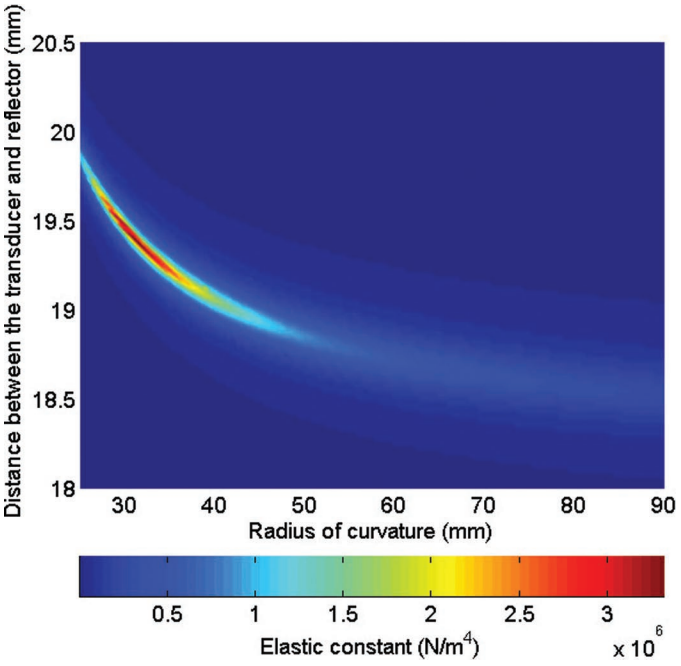

Fig. 10. Elastic constant as a function of distance d and radius of curvature R for the node near the reflector.

necessary to determine the distance d that produces the maximum elastic constant.

To verify the numerical model, the plane reflector was replaced by a curved reflector made of brass, with 30-mm radius of curvature. The replacement of a steel reflector by a brass reflector should not affect the levitator performance, because both materials have much higher specific acoustic impedance than air. The distance between the transducer and the reflector was set to 19.5 mm. To validate the numerical model, 2 small Styrofoam spheres were placed between the transducer and the curved reflector. The comparison between the acoustic potential and the equilibrium positions of the spheres is presented in Fig. 11. The elastic constant determined numerically for an applied voltage of 1 V corresponds to 1.8×10^6 N/m^4 for the bottom node and 2.7×10^6 N/m^4 for the top node. This result shows that a curved reflector can significantly increase the elastic constant over a levitator with a plane reflector. The elastic constant obtained with the curved reflector is 18 times higher than that obtained with a plane reflector with one levitation point ($d = 9$ mm) and 58 times higher in the levitator with 2 levitation points ($d = 18$ mm).

After levitating Styrofoam spheres, 2 steel spheres with a diameter of 2.5 mm were placed between the transducer and the curved reflector. The spheres equilibrium positions are shown in Fig. 12. Because of gravity, the steel spheres are located approximately 1.5 mm below the positions of minimum acoustic potential predicted by the finite element method. This difference was obtained by comparing the levitation positions of the steel spheres with that obtained with the Styrofoam spheres. It is assumed that the Styrofoam density is so small that it remains exactly at the minimum potential position. The presence of gravity can be easily modeled by adding a gravity term to the acoustic radiation potential.

IV. Transducer and Reflector Optimization

To reduce the electrical power necessary to levitate steel spheres, the finite element method is used to optimize both the transducer and the reflector design. In this section, the steel mechanical amplifier used in previous experiments is replaced by an aluminum mechanical amplifier with a curved radiating surface. The Langevin actuator (sandwich consisting of 2 aluminum loading masses and 4 piezoelectric ceramics) is not altered. The levitator parameters to be optimized are presented in Fig. 13. These parameters (L_1, L_2, R_1, R_2, R_3, and d) are optimized to generate 3 points of minimum potential. This number of levitation points was chosen to facilitate the access to the central levitation position.

A typical transducer design technique assumes that each transducer part can be considered as a half wavelength resonator. According to this design technique, if each transducer part has the same resonance frequency, the whole transducer should vibrate at this resonance frequency when the parts are joined together. In practice, the resonance frequency of the whole transducer does not

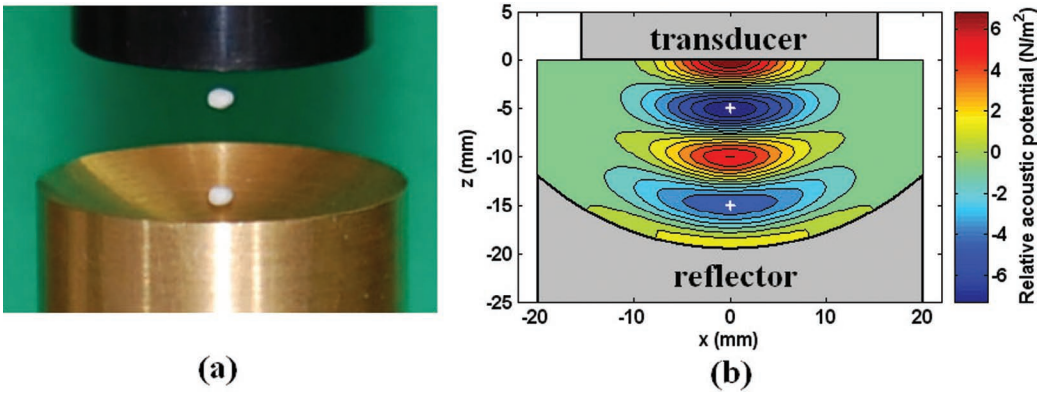

Fig. 11. Comparison between the numerical acoustic radiation potential and the levitation position of small Styrofoam spheres for the spherical reflector with 2 levitation points: (a) experimental and (b) numerical.

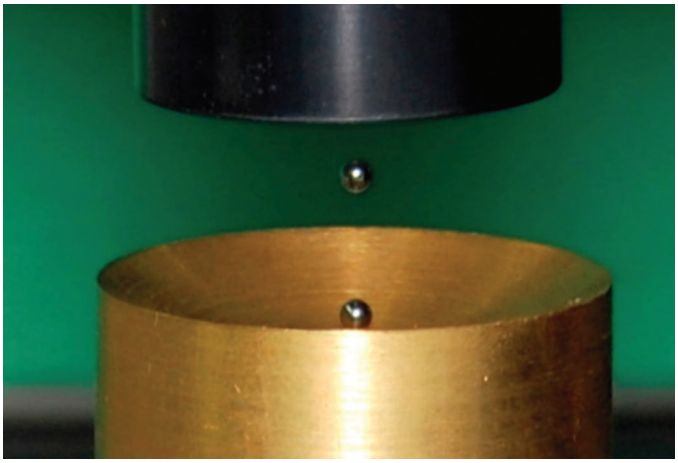

Fig. 12. Levitation of 2 steel spheres.

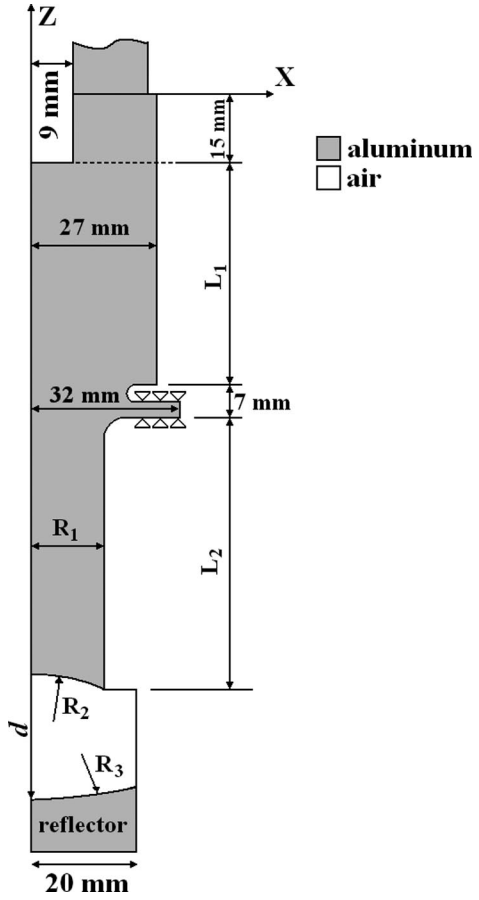

Fig. 13. Levitator parameters to be optimized.

exactly match the individual frequencies of each part, but it is a good start point to design the transducer. Using this technique, the first step in optimizing the levitator is to determine the resonance frequency of the Langevin actuator. The resonance frequency obtained through a harmonic analysis in ANSYS corresponds to 20 387 Hz. The mechanical amplifier parameters (L_1, L_2, R_1, and R_2) should be optimized while maintaining its resonance frequency near 20 387 Hz. It is also important to reduce the displacement at the transducer fixation point. This is necessary to avoid transmitting vibration to the structure where the transducer is fixed. The mechanical amplifier resonance frequency is obtained by using modal analysis in ANSYS. Table II presents a list with different mechanical amplifiers that have resonance frequency near 20 387 Hz and present small displacement amplitudes at the fixation point. This table also presents the resonance frequency for each mechanical amplifier.

A harmonic analysis was conducted in ANSYS to determine the resultant resonance frequency for each transducer. The resultant resonance frequency and displacement amplitude at the center of the radiating surface are presented in Table III. The comparison between the mechanical amplifiers resonance frequencies and the transducers resonance frequencies presented, respectively, in Tables II and III shows that the resultant resonance frequency slightly changes when the Langevin actuator is joined together with the mechanical amplifier. To find which transducer produces the maximum force on the levitated object, an optimization algorithm is used to determine the values of R_3 and d that maximize the elastic constant of the central levitation position for each transducer.

The flowchart of the optimization algorithm is presented in Fig. 14. In all simulations, it is considered that the initial material parameters are $R_3 = 30$ mm and $d = 28.5$ mm. In this work, it is used the Nelder-Mead Simplex Method to find the parameters R_3 and d that minimize an objective function. This method is available through the "fminsearch" function of Matlab optimization toolbox (MathWorks, Natick, MA) and the objective function is defined as the inverse of the elastic constant of the central levitation position. The optimization algorithm calls the package ANSYS at each iteration, and ANSYS returns the pressure field in the air region between the transducer and the reflector. The pressure field

TABLE II. List of Mechanical Amplifiers and Their Resonance Frequencies.

Mechanical amplifier	L_1 (mm)	L_2 (mm)	R_1 (mm)	R_2 (mm)	Resonance frequency (Hz)
1	48.5	59.5	10	100	20 403
2	48.5	55.5	15	100	20 466
3	48.5	56	15	50	20 433
4	42.5	58	18	50	20 385
5	42.7	58.2	18	40	20 410
6	43	58.5	18	35	20 410

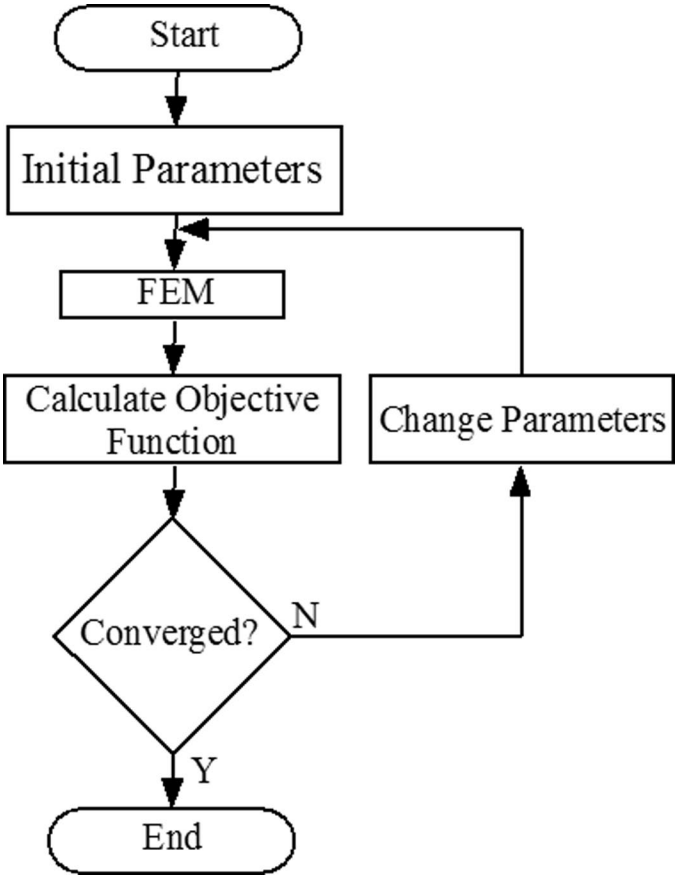

Fig. 14. Optimization algorithm flowchart.

is used to determine the acoustic radiation potential and consequently the elastic constant of the central levitation position. The values of R_3 and d that maximize the elastic constant are presented in Table IV for each ultrasonic transducer. According to this table, transducer number 6 produces the maximum elastic constant. The maximum elastic constant is obtained when the radius of curvature R_3 corresponds to 33.06 mm and the distance between the transducer and the reflector corresponds to 28.39 mm.

TABLE III. TRANSDUCER RESONANCE FREQUENCY.

Transducer	Resonance frequency (Hz)	Displacement amplitude (μm)
1	20 435	1.02
2	20 466	0.97
3	20 484	0.82
4	20 471	0.80
5	20 490	0.64
6	20 479	0.52

TABLE IV. PARAMETERS THAT MAXIMIZE THE ELASTIC CONSTANT $\tilde{k}$ OF THE CENTRAL LEVITATION POINT.

Transducer	R_3 (mm)	d (mm)	$\tilde{k}$ (N/m^4)
1	29.98	28.49	2.19×10^5
2	37.89	27.82	1.27×10^6
3	32.86	28.25	2.51×10^6
4	38.05	28.03	4.38×10^6
5	34.55	28.27	8.62×10^6
6	33.06	28.39	1.39×10^7

To verify the new levitator design, an aluminum mechanical amplifier was fabricated with the dimensions listed in Table II, line 6. It was also fabricated a curved aluminum reflector with a 33.0-mm radius of curvature. The new mechanical amplifier was connected to the Langevin actuator. This new ultrasonic transducer was placed at a distance of approximately 28.4 mm from the curved reflector and then 3 steel spheres were placed at the levitator. The comparison between the sphere's equilibrium position and the numerical acoustic radiation potential is presented in Fig. 15. Due to the superior concave surface, the top steel sphere cannot be seen in the picture of Fig. 15(a). The elastic constant of the central levitation position obtained with the new design is 92 times higher than that obtained with a plane reflector and only one levitation point. Comparing the new elastic constant with that obtained with a plane reflector operating with 3 levitation

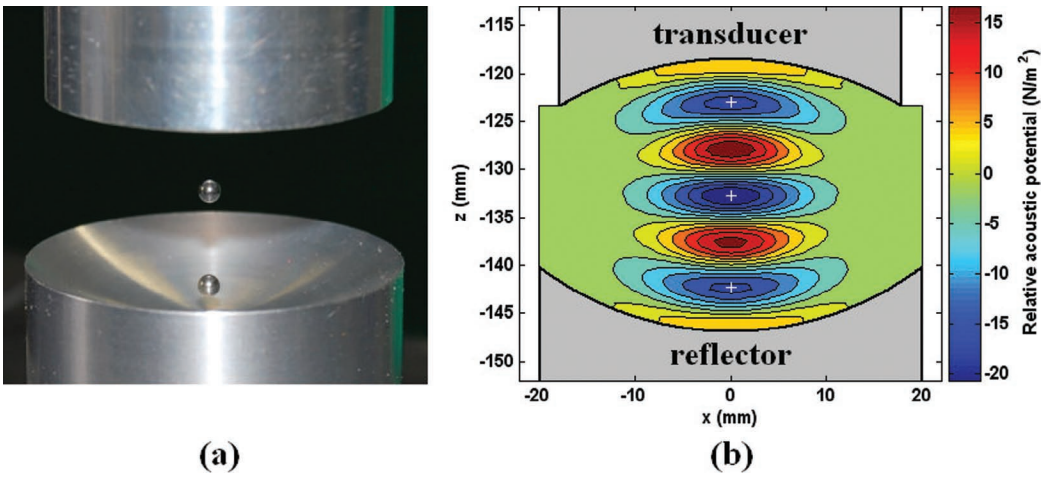

Fig. 15. Comparison between the numerical acoustic radiation potential and the levitation position of 3 steel spheres using the designed levitator: (a) experimental and (b) numerical.

points (d = 26.5 mm), the new elastic constant is 604 times higher than that obtained previously. To determine the minimum electric power consumption necessary to levitate the 3 steel spheres, the applied electric voltage is decreased until the spheres drop down into the reflector. The electrical power necessary to levitate the steel spheres is approximately 0.9 W.

V. Conclusion

This paper presented the finite element analysis of 3 configurations of single-axis acoustic levitators. The electrical impedance, the transducer face displacement, and the acoustic radiation potential predicted by the finite element showed good agreement with that obtained experimentally. The finite element method showed suitability to design an acoustic levitator with a concave reflector and concave radiating surface. The finite element method was used to determine the levitation force in levitators consisting of transducers with plane radiating surface and plane reflector, plane-faced transducer and concave reflector, and concave radiating surface transducer and concave reflector. It was shown that the best levitation force is obtained when both transducer and reflector have concave surfaces. When this levitator is operating with 3 levitation positions, the acoustic radiation force determined numerically is 604 times higher than that obtained with a plane-faced transducer and plane reflector. The new acoustic levitator allows levitating 3, 2.5-mm diameter steel spheres with a power consumption of only 0.9 W. Although the design of a single-axis levitator is relatively simple, this method can be very helpful in designing levitators with complex geometries.

Acknowledgments

We would like to thank João B. da Silva and Wellington Ramos for machining some transducer and levitator parts.

References

[1] Y. Tian, R. G. Holt, and R. E. Apfel, "A new method for measuring liquid surface tension with acoustic levitation," *Rev. Sci. Instrum.*, vol. 66, no. 5, pp. 3349–3354, 1995.

[2] R. Tuckermann, B. Neidhart, E. G. Lierke, and S. Bauerecker, "Trapping of heavy gases in stationary ultrasonic fields," *Chem. Phys. Lett.*, vol. 363, no. 3–4, pp. 349–354, 2002.

[3] S. Bauerecker and B. Neidhart, "Formation and growth of ice particles in stationary ultrasonic fields," *J. Chem. Phys.*, vol. 109, no. 10, pp. 3709–3712, 1998.

[4] S. Bauerecker and B. Neidhart, "Cold gas traps for ice formation," *Science*, vol. 282, no. 5397, pp. 2211–2212, 1998.

[5] S. Santesson and S. Nilsson, "Airborne chemistry: Acoustic levitation in chemical analysis," *Anal. Bioanal. Chem.*, vol. 378, no. 7, pp. 1704–1709, Apr. 2004.

[6] A. K. Geim, M. D. Simon, M. I. Boamfa, and L. O. Heflinger, "Magnet levitation at your fingertips," *Nature*, vol. 400, no. 6742, pp. 323–324, 1999.

[7] A. Ashkin and J. M. Dziedzic, "Optical levitation by radiation pressure," *Appl. Phys. Lett.*, vol. 19, no. 8, pp. 283–285, 1971.

[8] W. K. Rhim, S. K. Chung, D. Barber, K. F. Man, G. Gutt, A. Rulison, and E. Spjut, "An electrostatic levitator for high-temperature containerless materials processing in 1-g," *Rev. Sci. Instrum.*, vol. 64, no. 10, pp. 2961–2970, 1993.

[9] A. J. Rulison, J. L. Watkins, and B. Zambrano, "Electrostatic containerless processing system," *Rev. Sci. Instrum.*, vol. 69, no. 7, pp. 2856–2863, 1997.

[10] J. A. Gallego-Juárez, "Piezoelectric ceramics and ultrasonic transducers," *J. Phys. E Sci. Instrum.*, vol. 22, no. 10, pp. 804–816, 1989.

[11] C. R. Field and A. Scheeline, "Design and implementation of an efficient acoustically levitated drop reactor for in stillo measurements," *Rev. Sci. Instrum.*, vol. 78, no. 12, art. no. 125102, Dec. 2007.

[12] L. V. King, "On the acoustic radiation pressure on spheres," *Proc. R. Soc. Lond. A*, vol. 147, no. 861, pp. 212–240, 1934.

[13] L. P. Gor'kov, "On the forces acting on a small particle in an acoustical field in an ideal fluid," *Sov. Phys. Dokl.*, vol. 6, no. 9, pp. 773–775, 1962.

[14] M. Barmatz and P. Collas, "Acoustic radiation potential on a sphere in plane, cylindrical and spherical standing wave fields," *J. Acoust. Soc. Am.*, vol. 77, no. 3, pp. 928–945, 1985.

[15] W. J. Xie and B. Wei, "Parametric study of single-axis acoustic levitation," *Appl. Phys. Lett.*, vol. 79, pp. 881–883, 2001.

[16] W. J. Xie and B. Wei, "Dependence of acoustic levitation capabilities on geometric parameters," *Phys. Rev. E,* vol. 66, art. no. 026605, 2002.

[17] W. J. Xie, C. D. Cao, Y. J. Lü, Z. Y. Hong,, and B. Wei, "Acoustic method for levitation of small living animals," *Appl. Phys. Lett.,* vol. 89, art. no. 214102, 2006.

[18] E. H. Brandt, "Suspended by sound," *Nature*, vol. 413, no. 6855, pp. 474–475, Oct. 2001.

[19] T. Kozuka, K. Yasui, T. Tuziuti, A. Towata, and Y. Iida, "Acoustic standing-wave field for manipulation in air," *Jpn. J. Appl. Phys.*, vol. 47, no. 5, pp. 4336–4338, 2008.

[20] Vernitron Limited, "Measuring properties of piezoelectric ceramics," Southampton, UK, Bulletin 66011/B, 1976.

[21] L. E. Kinsler, A. R. Frey, A. B. Coppens, and J. V. Sanders, *Fundamentals of Acoustics*, 3rd ed. New York: Wiley & Sons, 1982.

[22] E. H. Trinh, "Compact acoustic levitation device for studies in fluid dynamics and material science in the laboratory and microgravity," *Rev. Sci. Instrum.*, vol. 56, no. 11, pp. 2059–2065, 1985.

Marco A. B. Andrade was born in São José dos Campos, São Paulo, Brazil, in 1981. He received the bachelor's degree in physics from the Instituto de Física, University of São Paulo, São Paulo, Brazil, in 2004 and the M.S. degree in mechanical engineering from Escola Politécnica, University of São Paulo, São Paulo, Brazil, in 2006. He is currently working toward the Ph.D. degree in mechanical engineering at Escola Politécnica. His research interests include acoustic levitation, modeling of piezoelectric transducers, and nonlinear acoustics.

Flávio Buiochi was born in São Paulo, Brazil, on June 21, 1965. He received the Dipl., M.S., and Ph.D. degrees in mechanical engineering from the Escola Politécnica, University of São Paulo, São Paulo, Brazil, in 1990, 1994, and 2000, respectively. He started his teaching career with the Department of Mechatronics Engineering, University of São Paulo, in 1992, where he is currently an assistant professor. From September 2001 to March 2003, he was a postdoctoral fellow with the Instituto de Acústica, Spanish Council Scientific Research. His research interests include the applications of ultrasonic transducers in nondestructive evaluation, the characterization of liquids and solids by ultrasound, and the development of ultrasonic piezoelectric and piezocomposite transducers.

Julio Cezar Adamowski (M'95) was born in Paraná, Brazil, on December 18, 1954. He received a degree in aeronautical mechanical engineering from the Instituto Tecnológico de Aeronáutica, São José dos Campos, Brazil, in 1980, an M.S. degree in precision machinery engineering from the Faculty of Engineering, University of Tokyo, Tokyo, Japan, in 1985, and a Ph.D. degree from the Escola Politécnica, University of São Paulo (EPUSP), São Paulo, Brazil, in 1993. He started his academic career with the Department of Mechanical Engineering, EPUSP, where he has been a full professor since 1998. He has been working on several research projects, including the ultrasonic characterization of materials, the ultrasonic pipeline inspection, applications of power ultrasonics, and ultrasonic transducers. His research interests include underwater modeling of elastic wave propagation in solids, piezoelectric transducers, ultrasonic characterization of materials, and ultrasonic nondestructive testing. Dr. Adamowski is a member of Acoustical Society of America (ASA).